Chaos

# Effects of mechano-electrical feedback on the onset of alternans: A computational study

Cite as: Chaos **29**, 063126 (2019); https://doi.org/10.1063/1.5095778
Submitted: 12 March 2019 . Accepted: 05 June 2019 . Published Online: 26 June 2019

Azzam Hazim, Youssef Belhamadia, and Stevan Dubljevic

# Effects of mechano-electrical feedback on the onset of alternans: A computational study

Cite as: Chaos **29**, 063126 (2019); doi: 10.1063/1.5095778
Submitted: 12 March 2019 · Accepted: 5 June 2019 ·
Published Online: 26 June 2019



Azzam Hazim,[1] Youssef Belhamadia,[2] and Stevan Dubljevic[3,a)]

## AFFILIATIONS

[1]Department of Biomedical Engineering, University of Alberta, Edmonton, Alberta T6G 2V2, Canada
[2]Department of Mathematics and Statistics, American University of Sharjah, Sharjah, United Arab Emirates
[3]Department of Chemical and Materials Engineering, University of Alberta, Edmonton, Alberta T6G 2V4, Canada

[a)]**Author to whom correspondence should be addressed:** stevan.dubljevic@ualberta.ca

## ABSTRACT

Cardiac alternans is a heart rhythm instability that is associated with cardiac arrhythmias and may lead to sudden cardiac death. The onset of this instability, which is linked to period-doubling bifurcation and may be a route to chaos, is of particular interest. Mechano-electric feedback depicts the effects of tissue deformation on cardiac excitation. The main effect of mechano-electric feedback is delivered via the so-called stretch-activated ion channels and is caused by stretch-activated currents. Mechano-electric feedback, which is believed to have proarrhythmic and antiarrhythmic effects on cardiac electrophysiology, affects the action potential duration in a manner dependent on cycle length, but the mechanisms by which this occurs remain to be elucidated. In this study, a biophysically detailed electromechanical model of cardiac tissue is employed to show how a stretch-activated current can affect the action potential duration at cellular and tissue levels, illustrating its effects on the onset of alternans. Also, using a two-dimensional iterated map that incorporates stretch-activated current effects, we apply linear stability analysis to study the stability of the bifurcation. We show that alternans bifurcation can be prevented depending on the strength of the stretch-activated current.



**Cardiac alternans is an abnormal heart rhythm that manifests as a sequence of alternating long and short action potential (AP) durations. It is a marker for cardiac arrhythmias and sudden death. In a cardiac cell model, the onset of alternans, which corresponds to a period-doubling bifurcation, can be induced when paced with a basic cycle length (BCL) less than a critical value. The direct physiological influence of cardiac contraction on excitation, referred to as mechano-electric feedback (MEF), is caused by a stretch-activated current, which can modulate the width (duration) of the AP (APD) in response to stretching. Here, we illustrate the effects of MEF on the APD for a range of BCLs, showing its antiarrhythmic effects close to the alternans bifurcation. In particular, we show that, depending on the strength of MEF, the critical BCL corresponding to the onset of alternans may be decreased.**

## I. INTRODUCTION

Under normal conditions at normal pacing rates, the electrically induced APs of excitable cardiac cells have similar durations. However, when pacing at a sufficiently high rate, the APD alternates between long and short values [Fig. 1(a)]. In tissue, this alternation can either be in phase (concordant alternans) or have parts that are out of phase with other parts of the tissue (discordant alternans). The APD alternans, which is characterized by a period-doubling bifurcation, has been shown to be a precursor of cardiac arrhythmias, some of which, such as ventricular fibrillation (VF), can lead to sudden cardiac death (SCD). Clinically, alternans are manifested as beat-to-beat fluctuations of T-wave amplitude, called T-wave alternans, on the electrocardiogram; this is an indicator of VF[1,2] and SCD risk. Therefore, prediction of the onset of period-doubling instability in cardiac tissue is of particular importance in detecting and preventing VF.

Mathematically, a one-dimensional (1D) iterated map[3,4] is usually used to characterize the APD alternans,

$$APD_{n+1} = f(DI_n). \tag{1}$$

Equation (1), known as APD restitution, relates the APD at the $n+1$th beat to the previous diastolic interval (DI) [Fig. 1(a)] (i.e., the time elapsed between the end of one AP and the beginning of the following one), where the BCL or simply the pacing period is held

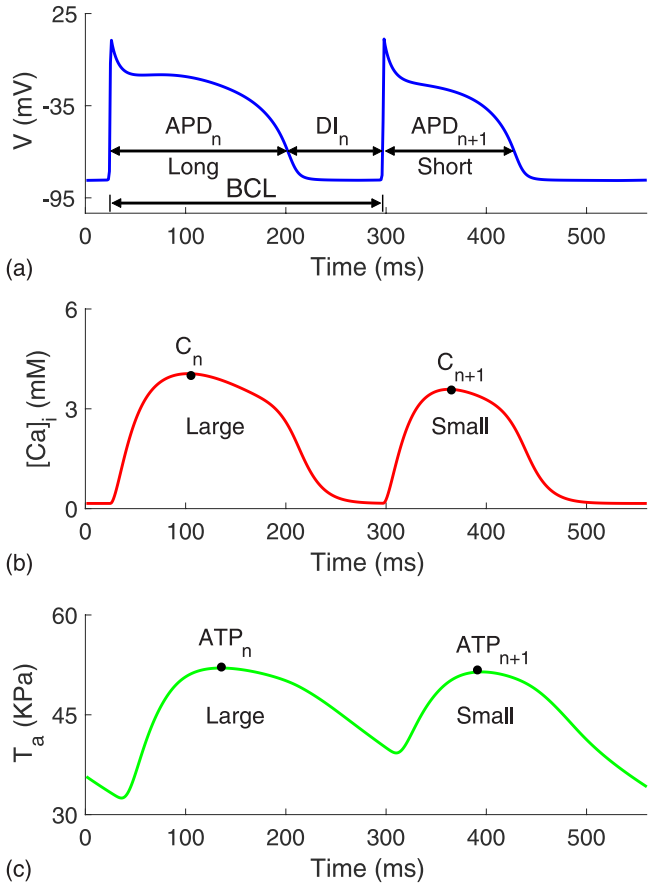


**FIG. 1.** Time evolution of voltage ($V$) (a), intracellular calcium concentration ($[Ca^{2+}]_i$) (b), and active tension ($T_a$) (c) of the cell in the middle of a cable of length $L$ = 7 cm in the Luo–Rudy I Niederer–Hunter–Smith (LR1NHS) model, when it is paced at the boundary with basic cycle length (BCL) = 272 ms and a steady state is reached.

constant so that BCL $= APD_n + DI_n$. Nolasco and Dahlen[3] were the first to show that whenever the slope of the APD restitution curve is greater than 1 (restitution hypothesis), a transition from normal heartbeat (period-1 rhythm) to alternans (period-2 rhythm) occurs. This was later formalized mathematically by Guevarra *et al.*[4] to show that the onset of alternans can be described as a period-doubling bifurcation, where the slope of the restitution curve corresponds to a derivative of the map (i.e., $df/d\mathrm{DI}$). Many theoretical and experimental studies have extended this theory using the iterated map approach and bifurcation theory to explain more complex phenomena, such as chaos,[5] in AP dynamics.

Many alternans studies still use this basic map representation, which assumes that modifications in DIs produce changes in APDs and that $df/d\mathrm{DI}$ determines the extent to which modifications in DIs produce APD alternans. However, many experimental studies have shown that the onset of APD alternans cannot always be predicted from the slope of the APD restitution; for example, in Hall *et al.*,[6] APD alternans was absent in frog heart muscle even though the restitution slope was significantly greater than 1. On the other hand, Dilly and Lab[7] observed alternans during ischemia, even though the slope was significantly less than 1. It can be concluded that the APD does not depend only on the previous DI, as described in Eq. (1), and that other factors influence the APD alternans. Important factors that have been extensively described in the literature include calcium cycling dynamics and cardiac memory. In cardiac myocytes, membrane voltage ($V$) and intracellular calcium concentration ($[Ca^{2+}]_i$) are bidirectionally coupled and, at the cellular level, alternans arises from an interplay of V and $[Ca^{2+}]_i$-cycling dynamics.[8–11] Hence, when the APD alternates, $[Ca^{2+}]_i$ alternates secondarily [see Figs. 1(a) and 1(b)] owing to voltage-dependent ionic currents (referred to as V $\rightarrow$ $Ca^{2+}$ coupling). Conversely, an alternation in $[Ca^{2+}]_i$ induces an alternation in the APD through calcium-sensitive ionic currents (referred to as $Ca^{2+}$ $\rightarrow$ V coupling). This latter coupling can be either positive (elevation in $[Ca^{2+}]_i$ lengthens the APD) or negative (elevation of $[Ca^{2+}]_i$ shortens the APD). Another factor with an important role is the pacing history of the cell; thus, the APD usually depends on the series of DIs preceding it and not just the immediately preceding DI, i.e., $APD_{n+1} = f(DI_n, DI_{n-1}, DI_{n-2}, \ldots)$. This phenomenon, known as cardiac memory,[12–16] is an intrinsic property of cardiac tissues. According to the theory of dynamical systems, the onset of alternans can be predicted from the eigenvalues of the map, i.e., bifurcation occurs when a characteristic eigenvalue leaves the unit circle through 1.[9,17]

In the heart, electrical waves propagate through cardiac tissue and initiate mechanical contraction. On the other hand, the deformations caused by contraction affect the electrical waves via the phenomenon of MEF.[18–21] It has been shown clinically that MEF can have both antiarrhythmic and proarrhythmic consequences.[22,23] Theoretical and experimental studies[24–33] have been performed to uncover the mechanisms of MEF and its effects on cardiac electrical activity. The results suggest that MEF may play an important part in arrhythmogenesis.[34,35] For instance, regions of substantial stretching induce large inward currents through stretch-activated channels (SACs) that can lead to conduction blocks, causing scroll wave breakup in these regions.[33] Conduction blocks can result in the initiation of reentry and fibrillation (see Refs. 36 and 37). Recent studies have shown that MEF may play a part in the restoration of normal cardiac electrophysiology.[38–41] In Opthof *et al.*,[38] the effect of the physiological left ventricular pressure pulse on ventricular repolarization was investigated using a Langendorff-perfused pig heart. It was demonstrated that with varying of the load in the left ventricle and the activation site, the normal ventricular pressure pulse tends to synchronize repolarization and, therefore, reduces susceptibility to ventricular arrhythmias. Also, a mechanical perturbation algorithm for controlling alternans via MEF has been presented.[39–41] It has been suggested that the amplitude of stretch-activated currents ($I_{sac}$) along a cable of 7 cm is modulated and applied during the repolarization of APs (between two predefined thresholds), when the control is activated, in order to suppress alternans.

One of the main effects of MEF results from $I_{sac}$ [defined in Eq. (10)], which when activated can alter the electrical properties of the myocardium via SAC.[19] Studies have investigated the effects of SAC during different phases of the AP, and the responses

vary depending on the timing of the mechanical stretch and the magnitude of $I_{sac}$.[22,25] This will result in delays after depolarizations or an AP (when the magnitude of $I_{sac}$ is above the threshold),[24,31,42–45] if stretching is applied during diastole. On the other hand, if stretching is applied during the plateau phase, it will alter repolarization of the AP,[23,45–49] leading to either shortening or lengthening of the AP; this change in the APD depends on the reversal potential[50] of the SAC, and the degree of shortening or lengthening of the APD is affected by the maximal conductance.[50] For instance, a mechanical induction occurring during the rat plateau, where the reversal potential of the SAC is near 0 mV, resulted in a prolonged APD,[46] while in guinea pig cells, with a high plateau and a lower reversal potential, a shortening of the APD was observed.[47] In addition, the stretch-induced changes in the APD and the degree of modulation are dependent on cycle length;[51,52] at long (short) cycle lengths, the APD is shortened (lengthened) under left ventricular loading by aortic occlusion. However, the mechanisms underlying the cycle-length-dependent effects of $I_{sac}$ on the APD remain to be elucidated.

In this work, we study the effects of MEF on the onset of alternans, illustrating the cycle length dependency of the stretch response and the effects of MEF on the APD, using a 1D electromechanical model of the heart. In particular, we show that MEF, depending on the strength of $I_{sac}$, may decrease the critical BCL ($BCL_{crit}$), which is the maximum BCL at which alternans occurs for this model when MEF is not present. Therefore, the influence of $I_{sac}$ on the APD at different BCL values is analyzed and discussed. To this end, we use a strongly coupled biophysically detailed electromechanical model of the heart, named the LR1NHS model, that accounts for the effects of electrical activity on the contraction and the effects of MEF on cardiac excitation. Phase one of the Luo–Rudy[53] model is used to represent the electrophysiological properties, while the mechanical properties of the passive myocardium are described using the Mooney–Rivlin material model.[41,54] The active tension ($T_a$) that couples the electrophysiological model to the cardiac mechanics model is generated using the Niederer–Hunter–Smith (NHS)[55] model. In addition, a 2D iterative map[41] that couples the AP and $T_a$ at the cellular level is utilized to illustrate the effects of MEF on the bifurcation point.

## II. METHODS

### A. The cardiac electromechanical model

A strongly coupled electromechanical model of cardiac tissue can be decomposed into four components, which are described in Secs. II A 1–II A 4.

#### 1. Mechanics model

Finite deformation theory is used to describe the mechanical deformation of cardiac tissue.[54,56] If a quasistatic equilibrium is assumed, deformation is described by the following equation:

$$\frac{\partial}{\partial X_M}(S^{MN}F_{jN}) = 0, \quad M,N,j = 1,2,3, \tag{2}$$

where $F_{jN} = (\partial x_i/\partial X_N)$ is the deformation gradient tensor ($\mathbf{F}$), with lower case and upper case indices corresponding to spatial (deformed) and material (undeformed) coordinates, respectively, and $S^{MN}$ is the second Piola–Kirchhoff stress tensor.

Myocardial properties include passive and active components. In this study, the active stress approach[54] is used to describe the active behavior of the myocardium. Therefore, $S^{MN}$ is given by

$$S^{MN} = S_p^{MN} + S_a^{MN}, \tag{3}$$

where $S_a^{MN}$ is the active stress generated by the electrical stimulations as described in Eq. (9) and $S_p^{MN}$ is the passive stress given by

$$S_p^{MN} = \frac{1}{2}\left(\frac{\partial W}{\partial C_{MN}} + \frac{\partial W}{\partial C_{NM}}\right), \tag{4}$$

where $C_{MN} = (\partial x_k/\partial X_M)(\partial x_k/\partial X_N)$ is the right Cauchy–Green deformation tensor ($\mathbf{C} = \mathbf{F}^T \cdot \mathbf{F}$). $W(I_1, I_2)$ is the strain energy function modeling the myocardium as a Mooney–Rivlin hyperelastic material[41,54] and is given by

$$W(I_1, I_2) = c_1(I_1 - 3) + c_2(I_2 - 3), \tag{5}$$

where $I_1(\mathbf{C}) = \mathrm{tr}(\mathbf{C})$ and $I_2(\mathbf{C}) = \frac{1}{2}(\mathrm{tr}(\mathbf{C}) - \mathrm{tr}(\mathbf{C}^2))$ are the first two principal invariants of $\mathbf{C}$, $\mathrm{tr}(\mathbf{C})$ is the trace of $\mathbf{C}$, and $c_1$ and $c_2$ are material constants.

#### 2. Electrophysiology model

The electrical activity in cardiac tissue is described by the monodomain model, which consists of a system of reaction-diffusion equations.[57] A modified version of this model[41,58] that takes into account the effects of MEF can be written as

$$\begin{aligned} C_m\frac{\partial V}{\partial t} &= \frac{1}{\sqrt{C}}\frac{\partial}{\partial X_M}\left(\sqrt{C}D_{MN}C^{NL}\frac{\partial V}{\partial X_L}\right) \\ &\quad - (I_{ion}(\mathbf{u}, V) + I_{sac}(\lambda, V) + I_{stim}), \\ \frac{d\mathbf{u}}{dt} &= \mathbf{f}(\mathbf{u}, V), \end{aligned} \tag{6}$$

where $V$ is the membrane voltage, $C_m$ is the membrane capacitance, $C = \det(C_{MN})$ (determinant of tensor $C_{MN}$), $t$ is the time, $D_{MN}$ are the components of the diffusion tensor, $C^{NL}$ are the components of the contravariant metric tensor (in an orthogonal material system, we have $C^{NL} = C_{NL}^{-1}$), $I_{ion}$ represents the ionic membrane currents, $\mathbf{f}$ is a prescribed vector-valued function, $\mathbf{u}$ is a vector of dependent states variable describing membrane gates and ionic concentrations $[Ca^{2+}]_i$ is one component of $\mathbf{u}$), $\lambda$ is the stretch [given in Eq. (8)], and $I_{stim}$ is the external stimulus current.

#### 3. Active tension model

The active tension, generated by the electrical activity and coupled to nonlinear elasticity equations describing deformation of the myocardium, is described by the NHS model.[55] This model, consisting of a nonlinear ordinary differential equation (ODE) system and describing the intracellular calcium dynamics and cross-bridge binding, can be written in its general form as

$$\begin{aligned} \frac{d\mathbf{w}}{dt} &= \mathbf{g}\left(\mathbf{w}, [Ca^{2+}]_i, \lambda, \frac{d\lambda}{dt}, T_a\right), \\ T_a &= h(\mathbf{w}), \end{aligned} \tag{7}$$

where **w** is a vector of internal state variables, **g** and $h$ are prescribed nonlinear functions (the precise form of **w**, **g**, and $h$ is given in the supplementary material), $[Ca^{2+}]_i$ is generated by the ionic model (given in Sec. II A 4), and $\lambda$ is the stretch (extension ratio) along the fiber direction, which is given by

$$\lambda = \sqrt{(\boldsymbol{n}^T \mathbf{C} \boldsymbol{n})}, \tag{8}$$

where $\boldsymbol{n}$ is the unit fiber direction in the undeformed configuration. Contraction of the heart results from the active tension, generated by electrical stimulation, and the $S_a^{MN}$ (introduced previously) corresponding to $T_a$ is given by

$$S_a^{MN} = T_a C^{MN}, \tag{9}$$

where $C^{MN}$ is the contravariant metric tensor.

#### 4. Ionic membrane model and stretch-activated currents

The functions $I_{ion}(\mathbf{u}, V)$ and $\mathbf{f}(\mathbf{u}, V)$ in the monodomain model [Eq. (6)] are given by the Luo–Rudy I (LR1) membrane model.[53] The LR1 model describes the electrophysiology of a ventricular cell from guinea pig and consists of six ionic currents and a system of eight ODEs including $[Ca^{2+}]_i$. The AP properties, including the APD alternans, of LR1 are mediated exclusively by $V$, since $[Ca^{2+}]_i$ passively follows the voltage. We modified the maximum conductance of the time-dependent potassium current to GK = 0.432 mS/cm$^2$, that of the sodium current to GNa = 16.0 mS/cm$^2$, and that of the slow inward current to Gsi = 0.06 mS/cm$^2$ in order to reduce the APD,[59,60] which was relatively large with the original parameter values, and to develop alternans at a shorter BCL.

Experimental studies[46,50,61] conducted on SAC have shown that $I_{sac}$ in the monodomain model [Eq. (6)] is induced when SAC is activated by mechanical stimulation and that the current-voltage relationship is almost linear. Therefore, linear models have been proposed[42,43,46,62–66] for $I_{sac}$ and have been used to study the effects of stretching on cardiac dynamics. Following these studies, $I_{sac}$ is modeled as in Ref. 58 and is given by

$$I_{sac} = G_s \frac{(\lambda - 1)}{(\lambda_{max} - 1)} (V - E_s), \tag{10}$$

where $\lambda$ is the stretch, given in Eq. (8), along the fiber direction and $\lambda_{max}$ is the maximal stretch, which we set to $\lambda_{max}$ =1.1 as in Ref. 58. $G_s$ is the maximal conductance and $E_s$ is the reversal potential. The value of $G_s$ is within the range 0–100 $\mu$S/$\mu$F.[19,67] For $E_s$, a range between −90 and 0 mV has been reported.[19,33,68] $I_{sac}$ is only present during stretching (i.e., when $\lambda > 1$), otherwise $I_{sac} = 0$.

### B. 1D mathematical model and numerical experiment setup

In this work, deformation was expressed with respect to the initial undeformed state. Therefore, all equations were expressed in terms of $X$ (material coordinates). In the 1D setting, $F_{11}$ (see Ref. 40) is given by

$$F_{11} = F = \partial x / \partial X, \tag{11}$$

where $x$ and $X$ are spatial and material coordinates, respectively. Let $x = X + u_d(X)$, where $u_d(X)$ is the displacement of a material point. Then, we can write $F$ as

$$F = \partial x / \partial X = 1 + \frac{\partial u_d(X)}{\partial X}. \tag{12}$$

Assuming that the cardiac fibers are parallel to the $X$-direction of the undeformed configuration, $\lambda$ [Eq. (8)] can be written as

$$\lambda = \sqrt{C_{11}} = F. \tag{13}$$

In one dimension, the equations that govern both the electrical and mechanical behavior of the heart muscle can be written as

$$C_m \frac{\partial V}{\partial t} = D \frac{\partial^2 V}{\partial X^2} - (I_{ion}(\mathbf{u}, V) + I_{sac}(\lambda, V) + I_{stim}), \tag{14}$$

$$\frac{d\mathbf{u}}{dt} = \mathbf{f}(\mathbf{u}, V), \tag{15}$$

$$\frac{d\mathbf{w}}{dt} = \mathbf{g}(\mathbf{w}, [Ca^{2+}]_i, \lambda, \frac{d\lambda}{dt}, T_a), \tag{16}$$

$$T_a = h(\mathbf{w}), \tag{17}$$

$$\frac{\partial}{\partial X} \left( \frac{T_a}{1 + \frac{\partial u_d(X)}{\partial X}} + 2(c_1 + 2c_2) \frac{\partial u_d}{\partial X} \right) = 0, \tag{18}$$

$$\lambda = F = 1 + \frac{\partial u_d(X)}{\partial X}, \tag{19}$$

$$I_{sac} = G_s \frac{(\lambda - 1)}{(\lambda_{max} - 1)} (V - E_s). \tag{20}$$

The electrophysiology model is given by Eqs. (14) and (15), where $D = D_{11}$ is the diffusion coefficient, the functions $I_{ion}(\mathbf{u}, V)$ and $\mathbf{f}(\mathbf{u}, V)$ are given by the LR1 model described in Sec. II A 4, and $I_{sac}$ is given by Eq. (20). The governing equations for the mechanical component are given by Eq. (18) (see Ref. 40 for derivation details), and those describing the excitation-contraction coupling (ECC) are given by Eqs. (16) and (17), where the functions **g** and $h$ are given by the NHS model. The electrophysiology equations [Eqs. (14) and (15)] are supplemented by no-flux boundary conditions corresponding to the assumption that the heart is electrically insulated. For the mechanical boundary conditions, we assume that both ends of the cable are fixed in space, modeling an isometric contraction regime, and, therefore, Eq. (18) is supplemented with zero displacement boundary conditions. Note that the dependence of the electrical conductivity (i.e., the diffusion tensor) on the mechanical deformation was not incorporated into the 1D model (see Sec. IV for details).

In all cardiac electromechanical simulations, a cable of length $L$ = 7 cm, fixed at its end points, is considered. The numerical schemes used to solve Eqs. (14)–(20) can be described as follows: (1) The derivatives were approximated with a semi-implicit finite difference method. The temporal derivative was replaced with a forward difference scheme, and the first and second spatial derivatives were replaced with the central difference and standard second-order central difference schemes, respectively. (2) The method of successive substitutions was used to transform the nonlinear boundary value problem [Eq. (18)] into a sequence of linear elliptic equations. We imposed no-flux boundary conditions for Eq. (14) ($\partial V / \partial X = 0$) and

**TABLE I.** Parameter values used for the simulations of the LR1NHS model.

| Description | Parameter | Value |
|---|---|---|
| Membrane capacitance | $C_m$ | 1 $\mu$F cm$^{-2}$ |
| Diffusion coefficient | $D$ | 0.001 cm$^2$ ms$^{-1}$ |
| Mooney–Rivlin constant | $c_1$ | 0.1 MPa |
| Mooney–Rivlin constant | $c_2$ | 0.05 MPa |
| Maximal stretch | $\lambda_{max}$ | 1.1 |

zero displacement boundary conditions at the fixed end points for Eq. (18) [$u_d(0) = 0$ and $u_d(L) = 0$]. An electrical and mechanical step size of $\Delta x = 0.025$ cm and electrical time step of $\Delta t = 0.01$ ms were employed in all simulations. The electrical stimulus was applied as square wave pulses with a magnitude of 80 $\mu$A/$\mu$F and a duration of 1 ms. The parameters of the active tension model [Eqs. (16) and (17)] are given in Ref. 55, and those used in Eqs. (14), (18), and (20) are given in Table I. Unless otherwise stated, we used values of $G_s = 15$ $\mu$S/$\mu$F and $E_s = -10$ mV and varied them to investigate the effects of these parameters on the APD and alternans.

The magnitude of the amplitude of the alternans is defined by

$$|a_n(\zeta)| = |APD_n(\zeta) - APD_{n-1}(\zeta)|, \tag{21}$$

where $n$ and $\zeta$ represent the beat number and space, respectively. The objective of this paper was to study the influence of MEF on the onset of alternans. Therefore, the set of Eqs. (14)–(20) that, together with the boundary conditions, constitute the LR1NHS model were solved numerically when the cable was paced at one end or in the middle with different BCLs and when MEF was applied or not [setting $G_s$ to zero in Eq. (20)]. The solution's behavior and $|a_n(\zeta)|$ are analyzed and discussed.

## III. RESULTS AND DISCUSSION

### A. Stretch distribution and its dependence on BCL

If a cable is paced (the first five cells are electrically stimulated) at one end with constant BCL, an electrical wave represented by $V$ propagates [Figs. 2(a)–2(d)] and generates $T_a$, which is triggered by an increase in the $[Ca^{2+}]_i$ from the electrical model, see Figs. 1 and 3. As can be seen in Fig. 1, when BCL = 272 ms was less than $BCL_{crit}$ = 276 ms ($BCL_{crit}$ is defined as the maximum BCL at which alternans occurs in the LR1NHS model when MEF is not present), an alternation in the APD occurred and induced an alternation in $[Ca^{2+}]_i$ through the mechanism of ECC, which in turn induced an alternation in the active tension peaks (ATPs) {defined as the highest value of $T_a$ within a beat [Fig. 1(c)]}; therefore, a long (short) APD corresponds to a large (small) ATP. As the wave propagated from the pacing site (PS) to the other end of the cable, the generated $T_a$ caused deformation of tissue; as a result, a stretch developed in the cable [Figs. 2(e)–2(h)]. As can be seen from Figs. 2(e)–2(h) and 4, if at any given time, some cells of the 1D cardiac cable are stretching ($\lambda > 1$), other cells are contracting ($\lambda < 1$), since, in an isometric setting, the cable's length remains fixed during mechanical contraction, meaning that the sum of $\lambda$ for all cells is equal to the length of the cable ($\int_0^L \lambda\, dX = L$). Moreover, the maximal values of stretch developed in the cable at different BCLs are not equal and decrease with BCL, see Figs. 2(e)–2(h) and 5. As can be seen in Fig. 2, the maximal value of stretch ($\lambda_{maxvs}$) decreases when BCL decreases from BCL = 800 ms to BCL = 276 (that corresponds to the onset of alternans when MEF is not present); the relation between BCL and $\lambda_{maxvs}$ is linear between BCL = 276 ms and BCL = 500 ms (see Fig. S1 in the supplementary material). This is because when BCL is decreased, the APD and, consequently, ATP decrease with BCL. Note that $\lambda$ depends on the $T_a$ [Eqs. (18) and (19)]; therefore, the magnitude, shape, and timing of deformation along 1D tissue depend on the magnitude, shape, and

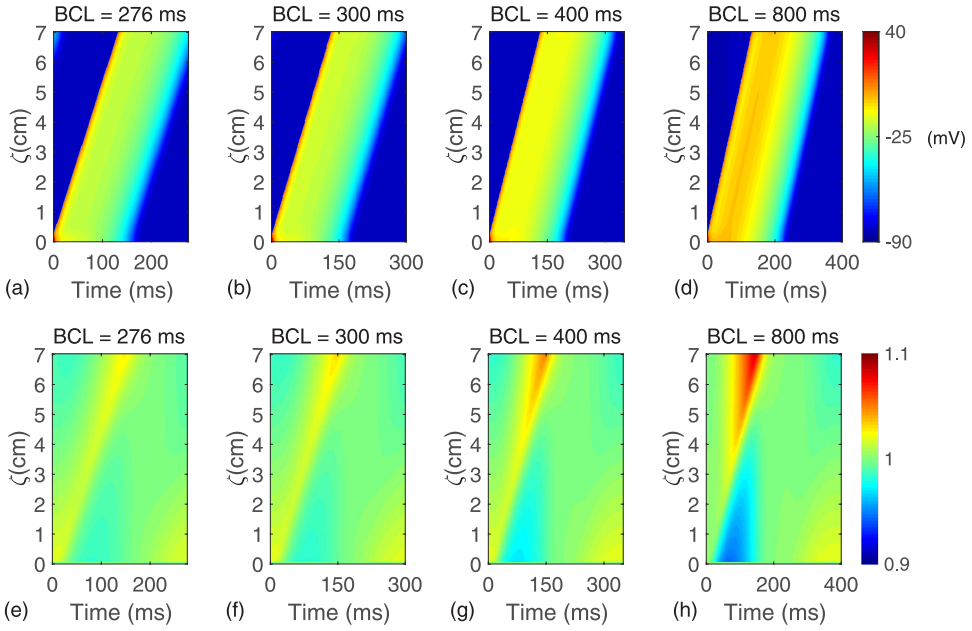


**FIG. 2.** (Top and bottom) Spatiotemporal evolution of $V$ and $\lambda$ in the LR1NHS model during one beat at steady state when a 7 cm cable of cardiac cells is paced at the boundary (first five cells) with four values of BCL [(a) and (e)] BCL = 276 ms, (b) and (f) BCL = 300 ms, (c) and (g) BCL = 400 ms, and (d) and (h) BCL = 800 ms], where BCL = 276 ms corresponds to the onset of alternans when MEF is not present.

time of activation and relaxation of mechanical contraction activity. In turn, $T_a$ depends mainly on the shape, activation, and relaxation time of the $[Ca^{2+}]_i$ of the ionic model used to represent the electrical activity of the cardiac cell. As can be seen in Figs. 2(e)–2(h) and 5, the stretch varies over time and its distribution along the cable is not symmetric if the cable is paced at the boundary ($x = 0$), see Figs. 2(e) and 2(g). In these figures, the cells that are closer to the other ends exhibit higher levels of stretch induced in the cable as a result of wave propagation, especially when BCL $\gg$ $BCL_{crit}$, compared with cells that are closer to the PS. One can conclude that stretching is not uniform along the cable and that it varies with BCL, with its magnitude decreasing when BCL decreases from 800 ms to $BCL_{crit}$ = 276 ms.

### B. Effects of MEF on the APD and alternans

$I_{sac}$, which is a function of $\lambda$ and $V$ [Eq. (20)], is considered to be the main effect of cardiac deformation on electrical activity. Therefore, the behavior of $\lambda$, which depends heavily on BCL, as discussed in Sec. III A, has a major role in determining the effects of $I_{sac}$ on the APD and alternans.

We start by illustrating the effect of MEF on the onset of alternans. To this end, APD alternans was induced in a 1D cable (the five leftmost cells were paced periodically with period $BCL_{crit}$ until a steady state was reached) under two conditions: with and without the presence of MEF. Therefore, two simulations were performed. In the first, $G_s$ was set to zero in Eq. (20), corresponding to one-way coupling (in which there is no influence of cardiac deformation on electrical activity). In the second, $G_s = 15\ \mu S/\mu F$, corresponding to two-way coupling (in which the influence of cardiac deformation on electrical activity is taken into account). In both simulations, we set $E_s = -10$ mV. For the first condition (MEF off), the cable was paced at the leftmost boundary, starting at BCL = 400 ms and gradually decreasing to BCL = $BCL_{crit}$ (i.e., for the onset of alternans). As can be seen in Fig. 6(a), APD alternans occurred when pacing with period BCL = 276 ms, which is the maximum BCL that allows alternans when MEF is off ($BCL_{crit}$ = BCL = 276 ms). When similar actions were performed in the presence of MEF (MEF on), no alternans occurred at $BCL_{crit}$ [Fig. 6(b)], and APD alternans occurred at BCL = 275 ms (simulation not shown). One can conclude that MEF has the effect of suppressing the APD alternans for a certain range of BCLs close to the $BCL_{crit}$. Note that the magnitude of alternans along the length of the cable was not uniform and it reached its minimum at the PS. Another numerical simulation that better illustrates the effects of MEF on the onset of alternans is shown in Fig. 6(c). This simulation was performed by excluding/including the MEF effects at specific times. As can be seen in Fig. 6(c), the alternans grew when MEF was not included and was suppressed by the inclusion of MEF, after which it regrew following the exclusion of MEF.

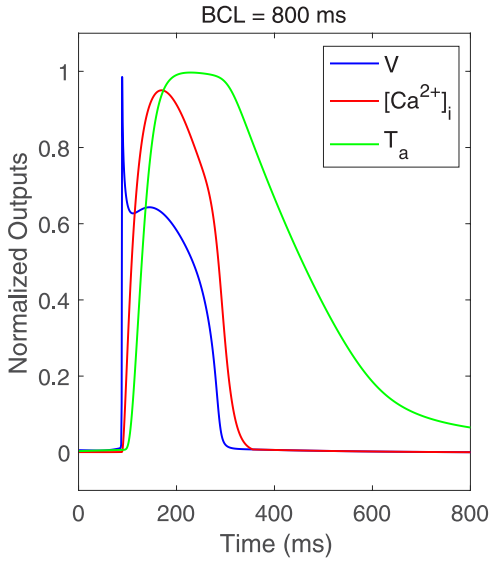


**FIG. 3.** Time evolution of normalized $V$ and $[Ca^{2+}]_i$ from the LR1 model and $T_a$ from the NHS model. The normalized outputs are given for the center cell in a 7 cm cable paced in the middle at BCL = 800 ms. As can be seen in this figure, there is a delay between the peak of the $T_a$ and the peak of the $V$, since $[Ca^{2+}]_i$ has to increase to a certain value before it can trigger the initiation of $T_a$.

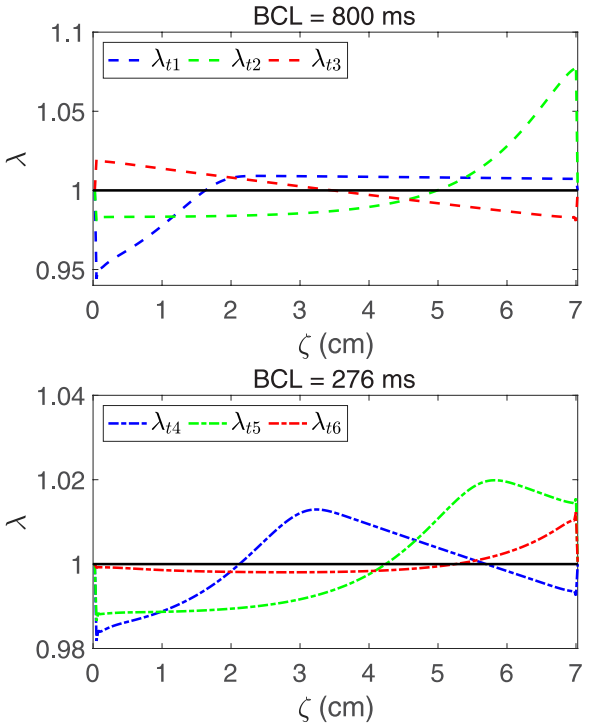


**FIG. 4.** Stretch distribution at three different times for the LR1NHS model at steady state when a 7 cm cable of cardiac cells, with both ends fixed, is paced at the boundary at BCL = 800 ms (top) and at BCL = 276 ms (bottom). $\lambda_{t_1}$ (blue dashed line), $\lambda_{t_2}$ (green dashed line), and $\lambda_{t_3}$ (red dashed line) are the stretches at times $t_1$ = 110 ms after the last electrical stimulus, $t_2 = (t_1 + 100)$ ms, and $t_3 = (t_1 + 350)$ ms, respectively, when BCL = 800 ms. $\lambda_{t_4}$ (blue dashed-dotted line), $\lambda_{t_5}$ (green dashed-dotted line), and $\lambda_{t_6}$ (red dashed-dotted line) are the stretches at times $t_4$ = 160 ms, $t_5 = (t_4 + 50)$ ms, and $t_6 = (t_4 + 100)$ ms, respectively, when BCL = 276 ms.

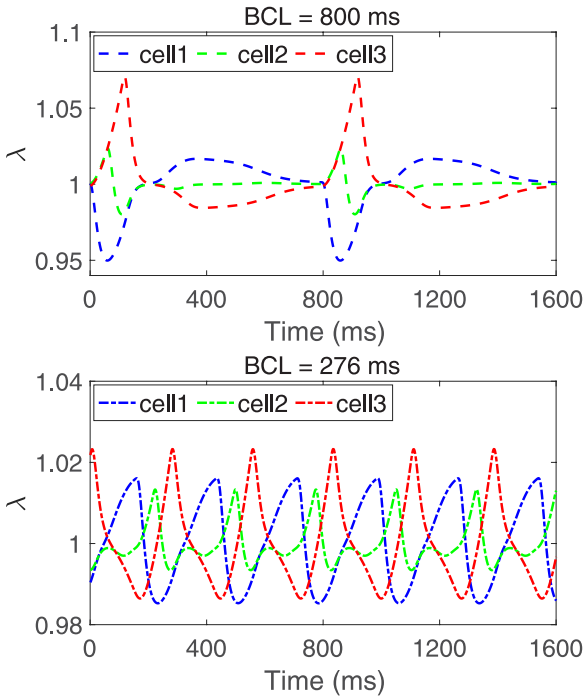


**FIG. 5.** Variation of stretch at three different cells for the LR1NHS model at steady state when a 7 cm cable of cardiac cells, with both ends fixed, is paced at the boundary at BCL = 800 ms (top) and at BCL = 276 ms (bottom). cell1, cell2, and cell3 are cells in the cable located at distance 0.5 cm, 3.5 cm, and 6.5 cm, respectively, from the pacing site (PS). Note that the time = 0 ms, which indicates the instant at which the recording begins in the top plot of this figure, corresponds to 40 ms after the last electrical stimulus for the three cells (dashed lines) while time = 0 ms in the bottom plot for the three cells (dashed-dotted lines) corresponds to 135 ms after the last electrical stimulus.

Before we could describe the influence of $I_{sac}$ on the APD, it was necessary to illustrate how λ varies during repolarization when BCL is changed. Therefore, we plotted λ and $V$ on the same figure for two BCLs (BCL = 800 ms and BCL = 276 ms). As can be seen in Fig. 7, the cells close to PS were mainly contracting during repolarization and stretching at the resting potential with BCL = 800 ms, while at BCL = 276 ms, they were stretching during early repolarization and early plateau phase and contracting afterward, then again stretching at the resting potential. On the other hand, cells that were close to the other cable end stretched during early repolarization and part of the plateau phase and contracted during late repolarization and at the resting potential with BCL = 800 ms, while at BCL = 276 ms they exhibited similar behavior to those with BCL = 800 ms, except that the magnitudes of the stretch were smaller, as discussed in Sec. III A. This has an important implication for the APD, as is discussed below.

We now investigate the effects of $I_{sac}$ on the APD for different BCLs. We start with the case of BCL = $BCL_{crit}$; therefore, λ, $I_{sac}$, and $V$ for BCL = 276 ms at steady state were plotted in Figs. 8(a) and 8(b) for two cells located at different positions. One cell (cell1; $\zeta = 1$ cm) was located close to the PS and the other (cell2; $\zeta = 6$ cm) close to the other cable end. Also, we assumed that the APD was measured using a voltage threshold corresponding to 90 ($APD_{90}$, i.e., the APD at 90% repolarization). As shown in Figs. 8(a) and 8(b), during early repolarization, $I_{sac}$ was an outward current and became an inward current when $V$ was below −10 mV. The $I_{sac}$ remained inward during the early plateau phase before reaching zero in the remaining part of the plateau phase and at late repolarization. Therefore, during early repolarization, $I_{sac}$ produces a hyperpolarizing effect facilitating repolarization (i.e., accelerates the rate of early repolarization), and then it produces a depolarizing effect delaying repolarization (i.e., slows the rate of repolarization); it has the same effect at the beginning part of the plateau phase, but no effect in the remaining part of the plateau phase or at late repolarization. This has the net effect of prolonging the short APD, and shortening the large APD, since the slowing process, which starts before the plateau phase, has enough time to increase the short but not the large. The reason is that, the plateau phase of the short APD is lower and shorter when compared with the large APD. Therefore, the relative time that $I_{sac}$ remains inward during the plateau phase of the short APD is greater than the one of the large APD. The restoration of normal APDs was mainly due to the effect of the inward current (the net effect of $I_{sac}$ on the large APD is small), which increased the short APD and caused, according to the restitution relation, a decrease in the large APD. The inward current in the case of cell2 [Fig. 8(b)] was more significant when compared to the one in cell1 [Fig. 8(a)]. Therefore, the increase (decrease) in the short (long) APD was larger in cell2 than in cell1. When $E_s = -30$ mV, $I_{sac}$ was always an outward current during repolarization and could not suppress alternans with the same value of $G_s$ (Fig. 9); for $E_s = 0$ mV, $I_{sac}$ during repolarization was almost entirely an inward current, which suppressed alternans for a smaller value of $G_s$ (Fig. 9). Note that when $I_{sac}$ is entirely an outward current during repolarization (the case where $E_s < -20$ mV), the suppression of alternans is feasible if the amplitude of $I_{sac}$ is large enough to decrease the large APD and then increase (according to the restitution relation) the short APD. When BCL is greater than $BCL_{crit}$, MEF has the effect of slightly shortening the APDs, and the mechanism of the effect of $I_{sac}$ on the APD is similar to the case of the large APD described earlier. When BCL is lower than $BCL_{crit}$, resulting in beat-to-beat alternation in the APD, the mechanism of the effects of $I_{sac}$ on the small and large APDs is similar to those when BCL = $BCL_{crit}$, which means it prolongs (shortens) the small (large) APD, see Figs. 8(c) and 8(d). As shown in Fig. 8(d) (at BCL = 270 ms and for the cell2), the large APD decreased by approximately 4.5 ms and the small APD increased by approximately 6 ms. As can be seen in Fig. 8, a large (small) APD corresponds to a large (small) amplitude of $I_{sac}$, since an alternation in the APD induces an alternation in the ATP through the mechanism of ECC; therefore, a large (small) APD corresponds to a large (small) ATP, which in turn induces an alternation in λ (large-small λ) for the same cell in the cable. Although alternans could not be suppressed at BCL = 270 ms when MEF was applied, the magnitude of its amplitude was decreased (see Fig. 10). This was because $|a_n(\zeta)|$ for the region close to PS when BCL = 270 ms was higher than that when $BCL_{crit}$ = 276 ms, and the strength of the $I_{sac}$ was not enough to account for the larger and smaller APDs. Moreover, the degree of alternation in stretching increased with BCL, and therefore the strength of $I_{sac}$ increased (decreased) with increasing (decreasing) λ (Fig. 8); consequently, the effects of $I_{sac}$ on the small APD decreased and its effects on the large

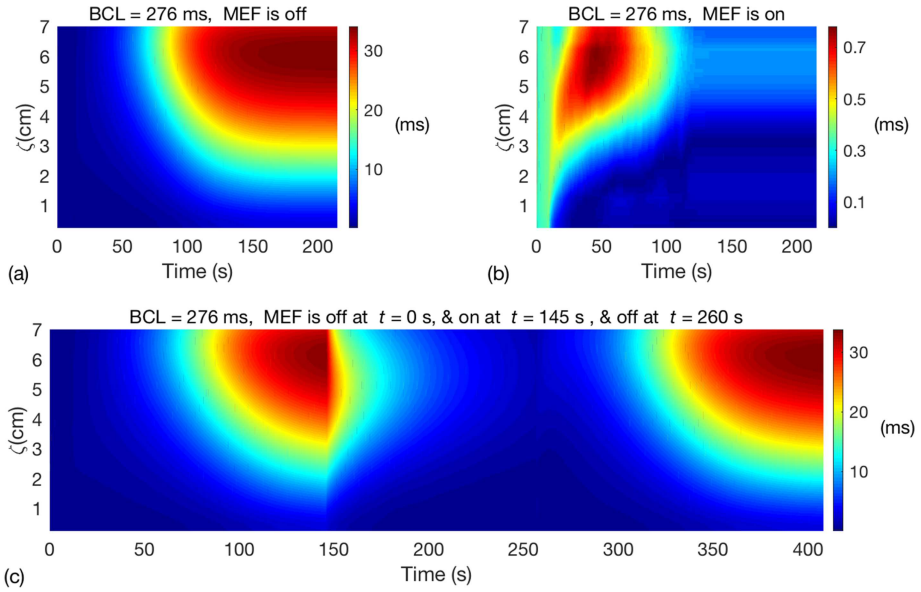


**FIG. 6.** Magnitude of the amplitude of the alternans [Eq. (21) where the APD was measured at 90% repolarization (APD90)], for the LR1NHS model without (a) and with (b) the presence of MEF, when a 7 cm cable of cardiac cells (the first five cells close to the PS which corresponds to $\zeta = 0$ cm) is paced at BCL = 400 ms and decreased gradually to $BCL_{crit}$ = 276 ms, which corresponds to the onset of alternans in (a) but not in (b). (c) Similar to (a), when MEF is turned off, alternans occurs when the cable is paced at $BCL_{crit}$ = 276 ms, but when MEF is turned on at time = 145 s, the APD alternans is suppressed and then starts to regrow again when MEF is turned off at 260 s.

APD increased slightly. In this way, the efficiency of $I_{sac}$ decreases with BCL and restoring normal APDs cannot be achieved unless $I_{sac}$ is modulated (see Ref. 41). As can be seen in Fig. 10, the effect of MEF on the APD and consequently on $|a_n(\zeta)|$ decreased as the BCL decreased, with a tendency to become arrhythmic at lower BCLs (see Sec. IV). Note that the effects of $I_{sac}$ on APDs were not equal for all cardiac cells along the cable, since $\lambda$ was not uniform along the cable length and also varied with BCL.

Two parameters of the $I_{sac}$ that have been shown to have important roles in the degree of lengthening and shortening of APDs are $G_s$ and $E_s$ {maximal conductance and reversal potential of $I_{sac}$ [Eq. (20)]}. The effects of $E_s$ on the onset of alternans (BCL = $BCL_{crit}$) are illustrated in Fig. 9. As can be seen in this figure, the efficiency of MEF decreased when $|E_s|$ increased (up to 20 mV), since, as stated before, the $I_{sac}$ changes during repolarization from almost inward at $E_s = 0$ mV to an outward current at $E_s = -20$ mV. On the other hand, if we change the value $G_s$, this will change the magnitude of $I_{sac}$ and its effects on APDs, which means that if $G_s$ is increased the $I_{sac}$ strength is increased, causing a decrease (increase) in the large (small) APD and thereby decreasing the $|a_n(\zeta)|$ (Fig. 11).

## C. Effects of MEF on period-doubling bifurcations

This section presents bifurcation diagrams obtained by numerical simulations for a single cardiac cell of the LR1NHS model that illustrate the effects of MEF on period-doubling bifurcation. A theoretical framework of iterative maps is also presented and used to analyze the simulation results.

### *1. Bifurcation diagrams for varying strengths of MEF*

In order to examine the effects of MEF on the period-doubling bifurcation, we plotted APD vs BCL (bifurcation diagram) for a cell-based LR1NHS model and for different strengths of $I_{sac}$. To this end, the cell in the middle of a 7 cm cable, which was selected to minimize the electronic and boundary (electrical and mechanical) effects, was paced at different BCLs, ranging from 350 ms to 260 ms, for three different values of $G_s$ (to regulate the strength of $I_{sac}$). Bifurcation diagrams (APD vs BCL) are given in Fig. 12. Note that, if the five

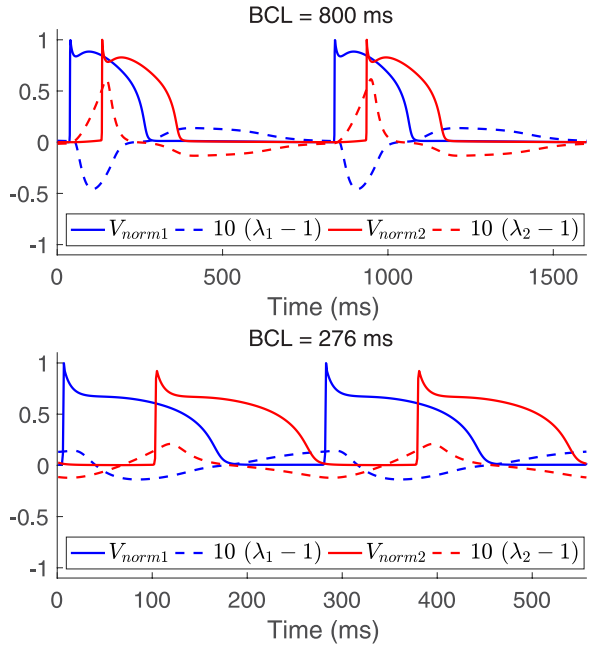


**FIG. 7.** Time evolution of normalized $V$ and 10 $(\lambda - 1)$ for two cells (cell1 and cell2) of the LR1NHS model at steady state when a 7 cm cable of cardiac cells is paced at BCL = 800 ms (top) or at $BCL_{crit}$ = 276 ms (bottom) in the presence of MEF. Cell1 (blue dashed line) and cell2 (red dashed line) are located at 1 cm and 6 cm, respectively, from the PS.

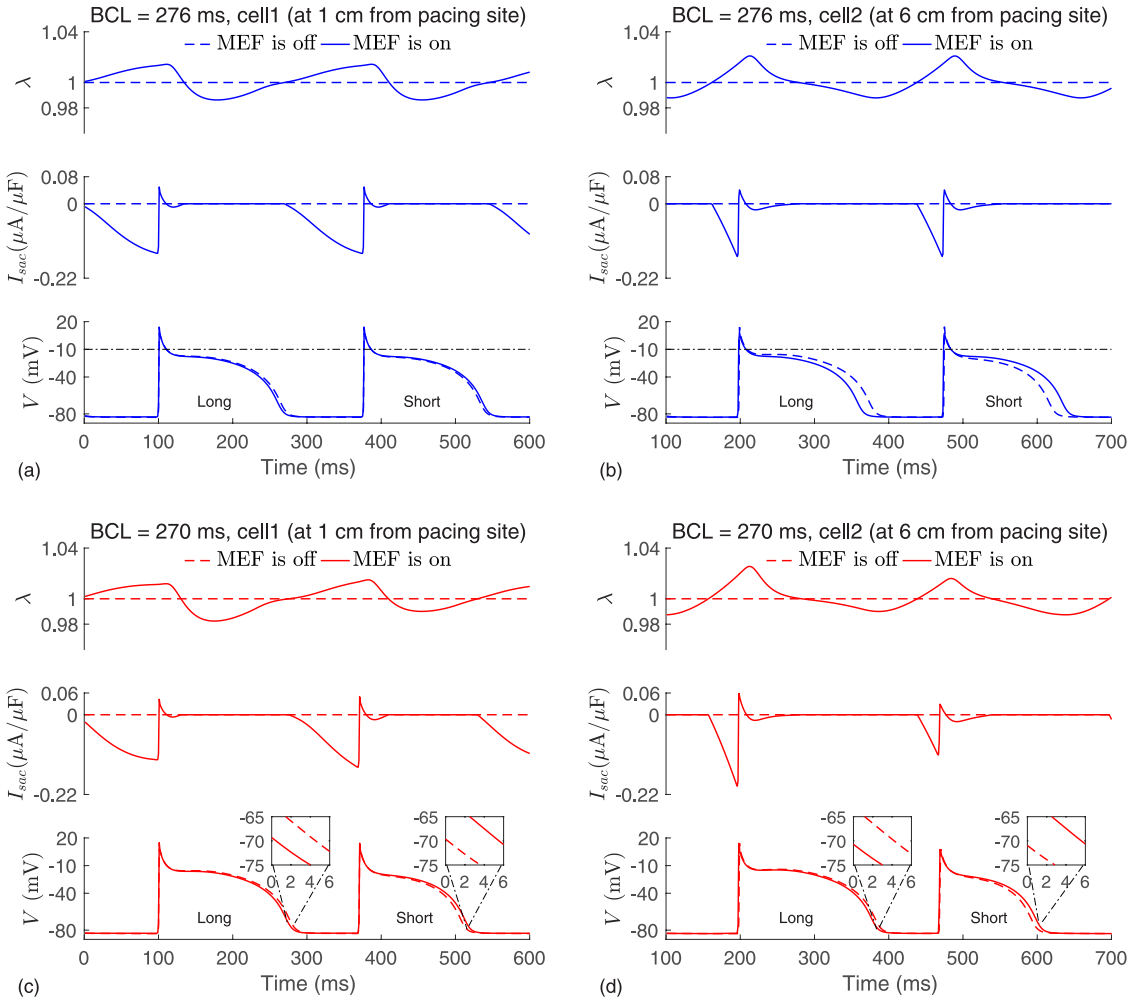


**FIG. 8.** (Left and right) Time evolution of λ (top), $I_{sac}$ (middle), and $V$ (bottom) for the cells positioned 1 cm (left) and 6 cm (right) from the PS, of the LR1NHS model, when a 7 cm cable is paced at the boundary with 400 ms and decreased gradually to either 276 ms or 270 ms, and then paced periodically with $BCL_{crit}$ = 276 ms [(a) and (b)] or BCL = 270 ms [(c) and (d)] until a steady state is reached.

cells in the middle of a 7 cm cable are paced with electrical stimulus of a magnitude of 80 $\mu A/\mu F$, the onset of alternans when MEF is not present corresponds to BCL = 276 ms (results not shown). The plot on the right-hand side of Fig. 12 is a zoomed-in version of the bifurcation diagrams that include the BCLs close to bifurcation points corresponding to the three values of $G_s$. As can be seen in this figure, for $G_s = 0\ \mu S/\mu F$ (no MEF is applied), the bifurcation point corresponds to BCL = $BCL_{crit} \approx 279$ ms, while for $G_s = 15\ \mu S/\mu F$ and $50\ \mu S/\mu F$, the new bifurcation points correspond to BCL ≈ 278 ms and BCL ≈ 276 ms, respectively. Therefore, with increasing $G_s$, the bifurcation point moves left, which means that APD alternans can be induced at higher pacing rates (lower BCLs) when $G_s$ is larger. Moreover, for all BCLs close to bifurcation points, corresponding to the three values of $G_s$, the $|a_n(\zeta)|$ are attenuated, and the attenuations decrease as BCL decreases. However, when pacing at BCL less than 240 ms, no effect of MEF on the $|a_n(\zeta)|$ was observed (bifurcation diagrams are shown in Fig. 12, for BCLs greater or equal to 265 ms, and Fig. S2 in the supplementary material, for BCLs between 240 ms and 265 ms), and the MEF effect became proarrhythmic when pacing at BCL ≪ $BCL_{crit}$.

### 2. Linear stability analysis

The effects of the MEF on the onset of instability is examined here using linear stability analysis. In our previous study,[41] we developed a 2D iterated map that couples the AP and $T_a$ at the cell level to incorporate the effects of MEF on the AP properties. In the development of this 2D map model, an approximation of λ (see Ref. 41)

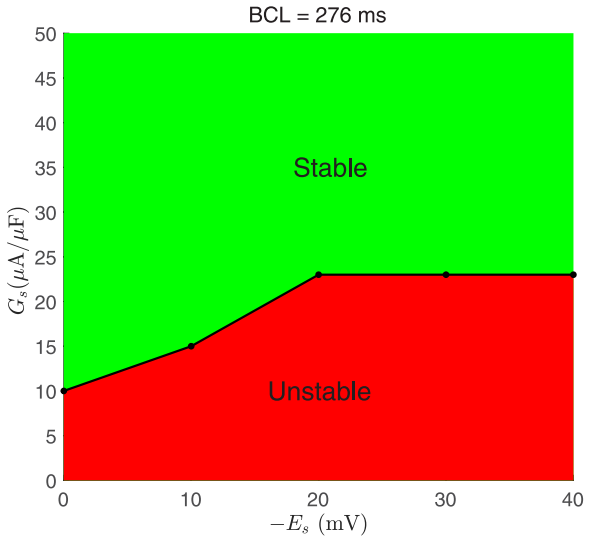


**FIG. 9.** Plot showing the stable and unstable regions of the ($G_s$, $E_s$) plane. The green region corresponds to the values of the parameters of $I_{sac}$ that suppress spatiotemporal alternans when a 7 cm cable is paced at the boundary with $BCL_{crit}$ = 276 ms and a steady state is reached.

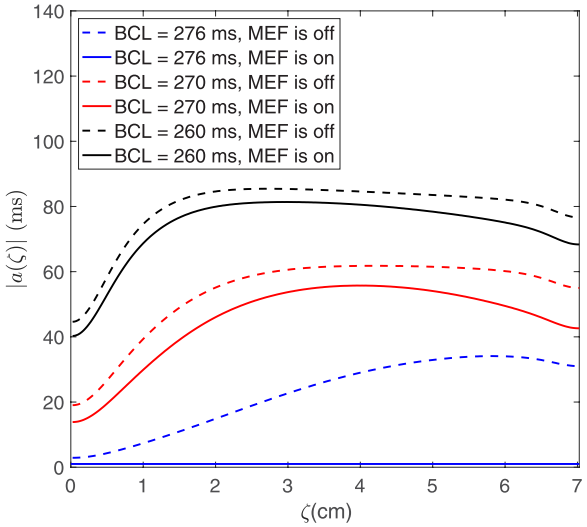


**FIG. 10.** Magnitude of the amplitude of alternans for the LR1NHS model at steady states, without MEF (dashed lines) and with MEF (solid lines), for four different BCLs, when a 7 cm cable is paced at the boundary with 400 ms and decreased gradually to BCL = 276 ms, 270 ms, or 260 ms, and then paced for 600 beats to its steady state. $APD_{90}$ (APD at 90% repolarization) was adopted as a measure of APD.

when $\lambda \leq 1.05$ is used, which is given by

$$\lambda \approx 1 + \frac{T_b - T_a(X)}{\tilde{c} - T_a(X)},$$

with

$$T_b \approx \frac{\int_0^L \frac{T_a(X)}{\tilde{c} - T_a(X)} dX}{\int_0^L \frac{1}{\tilde{c} - T_a(X)} dX}. \tag{22}$$

Hence, the $I_{sac}$, which is a function of $\lambda$ and $V$, is expressed instead in terms of $V$ and $T_a$ so that a bidirectional coupling between the $V$ and $T_a$ at the cellular level exists, and a 2D iterative map can be introduced (see Ref. 41). A slightly modified version of the 2D iterative map, which describes the beat-to-beat dynamics between the peak $T_a$ and the APD at beat $n$ to that at beat $n-1$, which is given by

$$\begin{aligned} APD_n &= F_1(APD_{n-1}, ATP_n), \\ ATP_n &= F_2(APD_{n-1}, ATP_{n-1}), \end{aligned} \tag{23}$$

where $ATP_n$ [Fig. 1(c)] is the ATP at beat $n$, measured from zero to the highest point in $T_a$, and $APD_n$ [Fig. 1(a)] is the width of $V$ at beat $n$, measured from the instant when $V$ crosses the threshold value on the wave front until the instant it falls below this value on the wave back. In Eq. (23), the APD at beat $n$ ($APD_n$) depends on the concurrent ATP ($ATP_n$) to express the effects of $I_{sac}$ on the repolarization of membrane voltage during a beat. The 2D iterated map will be used to study the stability of a fixed point $X_* = (APD_*, ATP_*)$ of the map, close to the alternans bifurcation at the cellular level for the cell-based model of LR1NHS (LR1NHSC). Note that, as described previously, $\lambda$ decreases from around 1 when a 7 cm cable of cardiac cells is paced at BCL = 800 ms to less than 0.05 when it is paced with BCL close to $BCL_{crit}$.

The stability of a fixed point $X_*$ can be obtained from linearization of the nonlinear map [Eq. (23)] in the vicinity of $X_*$ (see Ref. 41 for a detailed derivation),

$$\delta X_n \approx J\, \delta X_{n-1}, \tag{24}$$

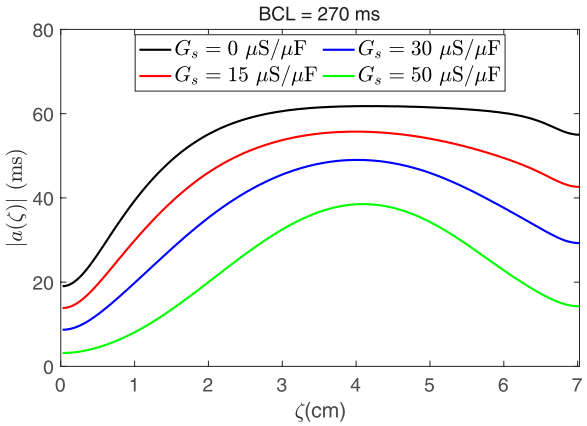


**FIG. 11.** Magnitude of the amplitude of alternans for the LR1NHS model at steady states for four different values of $G_s$, when a 7 cm cable is paced at the boundary with 400 ms and decreased gradually to 270 ms, and then paced periodically with BCL = 270 ms for 600 beats to its steady state. $APD_{90}$ (APD at 90% repolarization) was adopted as a measure of APD.

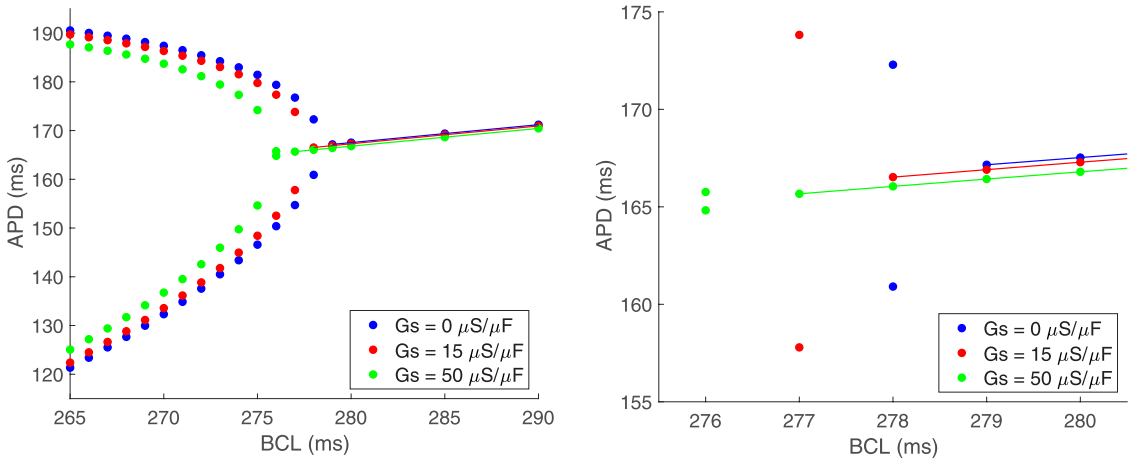


**FIG. 12.** Bifurcation diagrams showing APD vs BCL for different values of $G_s$ of the LR1NHS model (left panel) and a zoomed-in version of it (right panel). The cell in the middle of a 7 cm cable is paced with a periodic current wave form with a magnitude of 86 $\mu$A/$\mu$F and a duration of 1 ms for different BCLs, starting at BCL = 350 ms and decreasing by 1 ms, after a steady state is reached for each BCL, until BCL = 260 ms. This procedure was repeated for three values of $G_s$, and the simulation values of the APD at steady state are plotted vs BCL. APD at 90% repolarization was adopted as a measure of APD.

where $\delta X_{n-1} = X_{n-1} - X_*$ is a small perturbation from the fixed point and $J = J(X_*)$ is the Jacobian matrix evaluated at $X_*$, which is given by

$$J = \begin{pmatrix} \frac{\partial APD_n}{\partial APD_{n-1}} + \frac{\partial APD_n}{\partial ATP_n}\frac{\partial ATP_n}{\partial APD_{n-1}} & \frac{\partial APD_n}{\partial ATP_n}\frac{\partial ATP_n}{\partial ATP_{n-1}} \\ \frac{\partial ATP_n}{\partial APD_{n-1}} & \frac{\partial ATP_n}{\partial ATP_{n-1}} \end{pmatrix}. \quad (25)$$

The eigenvalues of $J$ determine the stability of $X_*$ to small perturbations. If all the eigenvalues of $J$ have magnitude less than 1, the fixed point $X_*$ is stable and the onset of instability corresponds to the largest absolute value of the eigenvalues passing through the unit circle. This instability gives rise to a period double bifurcation corresponding to alternans. To calculate the eigenvalues of $J$, we need first to evaluate the terms of the Jacobian matrix at the fixed point of the map, which corresponds to a period-1 rhythm, close to the alternans bifurcation. We start by rewriting the matrix $J$ as

$$J = \begin{pmatrix} R + c\,A & c\,B \\ A & B \end{pmatrix}, \quad (26)$$

where $R = \frac{\partial APD_n}{\partial APD_{n-1}}$, $A = \frac{\partial ATP_n}{\partial APD_{n-1}}$, $B = \frac{\partial ATP_n}{\partial ATP_{n-1}}$, and $c = \frac{\partial APD_n}{\partial ATP_n}$. The term $c$, which measures the dependence of the voltage on the active tension, can also be considered a measure of the MEF coupling effects, since in the LR1NHSC model, $I_{sac}$ is a function of $V$ and $\lambda$, which in turn is a function of $T_a$ [Eq. (22)]; therefore, the effects of $I_{sac}$ on the APD depend explicitly on ATP. In order to evaluate $c$, $G_s$ was varied between 0 and 100 $\mu$S/$\mu$F to account for the strength of the $I_{sac}$. The evaluations of terms $R, A, B$, and $c$ at the fixed point of the map [Eq. (23)] are given in Figs. 13 and 14. The BCL was chosen so that, when MEF was not applied, the cell, which was paced at BCL, exhibited period-1 dynamics but very close to the bifurcation point ($R \approx -1$). For the case of $G_s = 0$, we have $c = 0$, which corresponds to $I_{sac} = 0$ (MEF off), and the eigenvalues of matrix $J$ are $B$ and $R$, and, since $|R| = 1$, the fixed point $X_*$ undergoes a period-doubling bifurcation. For the general case when $c$ is not zero (MEF on and its strength depends on the value of $G_s$), the stability of the system [Eq. (23)] is governed by the eigenvalues of matrix $J$, which are given by

$$\lambda_1 = \frac{1}{2}\left(R + c\,A + B + \sqrt{(R + c\,A + B)^2 - 4\,R\,B}\right),$$
$$\lambda_2 = \frac{1}{2}\left(R + c\,A + B - \sqrt{(R + c\,A + B)^2 - 4\,R\,B}\right). \quad (27)$$

The values of $c$ when $G_s$ is within the range of 0–100 $\mu$S/$\mu$F and the eigenvalues $\lambda_{1,2}$ varying with $G_s$ are sketched in Fig. 14. As can be seen in the figure, the magnitude of $c$ (magnitude of the strength of MEF coupling effects) increased when $G_s$ increased. Figure 14 shows that $|\lambda_2|$ (the absolute value of the largest eigenvalue of $J$) decreased when $G_s$ increased. Therefore, as $G_s$ increases, the strength of the $I_{sac}$ increases and the period-doubling bifurcation point moves further right, effectively stabilizing the branch of unstable fixed points located close to the bifurcation point in the region of period-2 rhythm.

## IV. LIMITATIONS

All numerical simulations were performed under the assumption that the alternans was voltage driven (caused by voltage instability). Although this has been widely assumed in the literature, APD alternans can also be induced by calcium-driven instability (caused by the instability of intracellular calcium cycling). Complex behaviors are possible in the latter case, depending on the strength of the calcium-driven instability and the nature of $Ca^{2+} \rightarrow V$ coupling.[8–10]

In this work, we only considered isometric conditions (where both ends of the cable are fixed in space). This affects the distribution

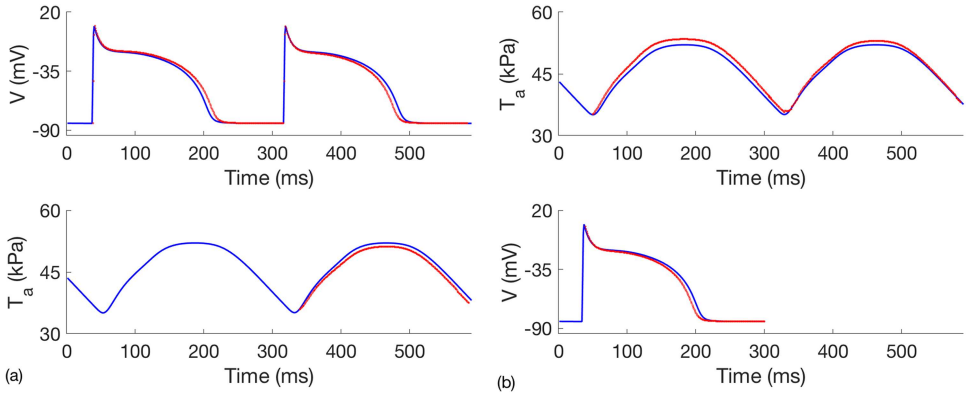


**FIG. 13.** Evaluations of the terms $R$, $A$, $B$, and $c$ at the fixed point of the map [Eq. (23)]. To this end, the cell in the middle of a cable of length $L$ = 7 cm is paced at BCL = 279 ms until steady state is reached (blue line). (a) $R = \partial APD_n/\partial APD_{n-1} = -\partial APD_n/\partial DI_{n-1}$ (restitution relation) and $A = \partial ATP_n/\partial APD_{n-1}$ ($V \rightarrow T_a$ coupling between the APD at a given beat and the ATP on the next beat) were evaluated as follows: a slight increase of the APD (red line) at a given beat from its steady state position (blue line) leads to a decrease in APD (red line) and ATP (red line) at the next beat (due to a shortening of the DI). $R$ and $A$ were evaluated by dividing the resulting decreases of APD and ATP, respectively, by the size of the initial increase of APD ($R \approx -1$ and $A \approx -0.13$). (b) $B = \partial ATP_n/\partial ATP_{n-1}$ and $c = \partial APD_n/\partial ATP_n$ ($T_a \rightarrow V$ coupling between the ATP and the APD at a given beat) were evaluated as follows: a slight increase of the ATP (red line) at a given beat from its steady state position (blue line) leads to an increase in ATP (red line) at the next beat and to a decrease in APD (red line) at the same beat (the $T_a \rightarrow V$ coupling is negative in this model). $B$ was evaluated by dividing the resulting increase in ATP by the size of the initial increase in ATP ($B \approx 0.02$), and $c$, which depends on the value of $G_s$ chosen, is plotted vs $G_s$ in Fig. 14.

of stretching along the cable, as if muscle fibers are stretched in some regions of the cable, the fibers will be compressed in other regions so that the length of the cable remains constant. For the isotonic case (boundary loading conditions), no constraint is imposed on the cable length; therefore, a change in the stretch distribution may occur. This may change how $I_{sac}$ affects the APD and, consequently, its effects on the onset of alternans.

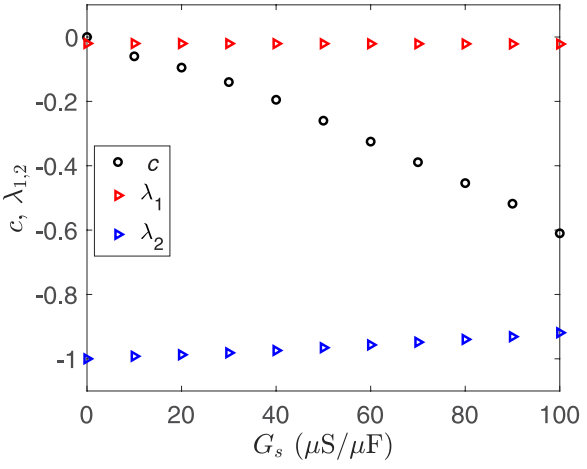


**FIG. 14.** The strength of the MEF coupling effects ($c$) and eigenvalues ($\lambda_{1,2}$) [Eq. (27)] of $J$ [Eq. (26)] are plotted vs $G_s$. $\lambda_{1,2}$ are plotted vs $G_s$ since they are functions of $c$, which in turn is a function of $G_s$. Increasing $G_s$ increases the magnitude of the strength of $c$, and the largest eigenvalue in absolute value ($|\lambda_2|$; blue triangle) decreases from $|\lambda_2| = 1$ when $G_s = 0\ \mu S/\mu F$ to $|\lambda_2| \approx 0.9$ when $G_s = 100\ \mu S/\mu F$.

Conduction velocity (CV) restitution, which refers to the dependence of the CV of the AP on the preceding DI, along with the APD restitution curves, has been shown to have an effect on alternans.[69] Similar to other studies,[33,70] we found that the influence of MEF on the CV depends on BCL, $G_s$, and $E_s$, although it can be neglected for the values used in the LR1NHS model. However, for large values of $G_s$ ($G_s > 50\ \mu S/\mu F$), the myocardial stretch increased the CV, which, along with APD restitutions and lower BCL (BCL $\ll$ $BCL_{crit}$), has a critical role in discordant alternans (see Fig. S3 in the supplementary material). On the other hand, the dependence of conductivity on mechanical stretching was not included in this study. A change in the conductivity could modify the CV, which plays a part in the development of alternans. However, with or without the inclusion of the effects of stretching on diffusion, the onset of alternans can be shifted to lower BCLs with an appropriate selection of the parameters of $I_{sac}$ ($G_s$ and $E_s$).

## V. CONCLUSIONS AND FUTURE WORKS

This study investigated numerically and theoretically the effects of MEF on the onset of alternans. The numerical results were obtained using a 1D biophysically detailed electromechanical model of cardiac tissue. As demonstrated in this work, the distribution of stretching along the cable is not uniform and the stretch magnitude, which varies with BCL, is larger at BCL $\gg$ $BCL_{crit}$. Therefore, the stretch behavior along with the parameters $G_s$ and $E_s$ determines the effect of $I_{sac}$ on the APD. In addition, a theoretical framework of 2D iterative maps that incorporate the effects of $I_{sac}$ was used to demonstrate the MEF effects on the period-doubling bifurcation, corresponding to the onset of alternans in a single cardiac cell. In particular, we showed that $BCL_{crit}$ can be shifted to lower values, where the degree of this shift depends on the strength of $I_{sac}$. The antiarrhythmic effects of MEF was demonstrated using the LR1

model representing electrophysiological properties with the NHS model for active tension generation. Calcium-sensitive currents, such as the $L$-type calcium current ($I_{CaL}$) and sodium-calcium exchange current ($I_{NaCa}$), are not included in the LR1 model. However, we believe that if the alternans is voltage driven, the presence of these currents will not reverse the effects of $I_{sac}$, which is also a calcium dependent current, on the APD. For example, in the FOX model,[71] these currents are included in this model, the alternans was suppressed when a modulated $I_{sac}$ was applied.[41] But, if the APD alternans is calcium-driven, the situation is complex since the $I_{CaL}$ and $I_{NaCa}$, which can prolong or shorten the APD, can have opposite effects and the net effect depends on the relative contributions of these currents to the APD.[8,9] We expect the effectiveness and efficiency of MEF on the onset of alternans, that mainly depend on the AP and $[Ca^{2+}]_i$ dynamics, to vary among cell species. For example, myocytes of larger mammals, including humans, have longer APs than ones observed in smaller mammals such as rat and mouse. The AP and $[Ca^{2+}]_i$ dynamics affect the profile of $T_a$ and consequently, the distribution of mechanical stretch which plays the main role in APD changes.

The interaction between the mechanical and electrical events in the heart can be depicted as a simple closed-loop feedback control system, where the mechanical stretch can stabilize the electrical activity of the heart via MEF and in the vicinity of the alternans bifurcation. However, a potential role of MEF in arrhythmogenesis can be shown if a 7 cm cable of cardiac cells of the LR1NHS model (but with larger magnitude values of $G_s$ and $E_s$) is paced at lower BCLs (BCL $\ll$ $BCL_{crit}$). This is because the nonuniform distribution of stretching produces, via SAC, a spatial dispersion in electrophysiological properties by converting an existing state of concordant alternans to discordant alternans. The latter state is considered to be very arrhythmogenic, since it increases the dispersion of repolarization and can result in a localized block.[72,73] The results are beyond the scope of this paper but will be the subject of future work.

## SUPPLEMENTARY MATERIAL

See the supplementary material for a summary of the equations of the NHS model (the NHS model is used to generate active tensions) and Figs. S1–S3, which show the variation of the maximal values of stretch vs BCL (Fig. S1), bifurcation diagrams showing APD vs BCL for different values of $G_s$ of the LR1NHS model when BCL varies between 240 ms and 265 ms (Fig. S2), and spatiotemporal evolution of $V$ in the LR1NHS model with $G_s = 0\,\mu S/\mu F$ (top), with $G_s = 52\,\mu S/\mu F$ and $E_s = -20$ mV (bottom), and with BCL = 210 ms (Fig. S3).

## ACKNOWLEDGMENTS

The authors acknowledge the Natural Science and Engineering Research Council of Canada (NSERC) for financial support. Y. Belhamadia gratefully acknowledges the American University of Sharjah Enhanced Faculty Research Grant.

## REFERENCES

[1] D. S. Rosenbaum, L. E. Jackson, J. M. Smith, H. Garan, J. N. Ruskin, and R. J. Cohen, "Electrical alternans and vulnerability to ventricular arrhythmias," New Engl. J. Med. **330**, 235–241 (1994).
[2] J. M. Pastore *et al.*, "Mechanism linking t-wave alternans to the genesis of cardiac fibrillation," Circulation **99**, 1385–1394 (1999).
[3] J. B. Nolasco and R. W. Dahlen, "A graphic method for the study of alternation in cardiac action potentials," J. Appl. Physiol. **25**, 191–196 (1968).
[4] M. R. Guevara, G. Ward, A. Shrier, and L. Glass, "Electrical alternans and period doubling bifurcations," IEEE Comp. Cardiol. **562**, 167–170 (1984).
[5] D. R. Chialvo, R. F. Gilmour, Jr., and J. Jalife, "Low dimensional chaos in cardiac tissue," Nature **343**, 653–657 (1990).
[6] G. M. Hall, S. Bahar, and D. J. Gauthier, "Prevalence of rate-dependent behaviors in cardiac muscle," Phys. Rev. Lett. **82**, 2995–2998 (1999).
[7] S. G. Dilly and M. J. Lab, "Electrophysiological alternans and restitution during acute regional ischaemia in myocardium of anaesthetized pig," J. Physiol. **402**, 315–333 (1988).
[8] Y. Shiferaw, D. Sato, and A. Karma, "Coupled dynamics of voltage and calcium in paced cardiac cells," Phys. Rev. E **71**, 021903 (2005).
[9] Y. Shiferaw and A. Karma, "Turing instability mediated by voltage and calcium diffusion in paced cardiac cells," Proc. Natl. Acad. Sci. U.S.A. **103**, 5670–5675 (2006).
[10] D. Sato, Y. Shiferaw, A. Garfinkel, J. N. Weiss, Z. Qu, and A. Karma, "Spatially discordant alternans in cardiac tissue: Role of calcium cycling," Circ. Res. **99**, 520–527 (2006).
[11] Z. Qu, Y. Shiferaw, and J. N. Weiss, "Nonlinear dynamics of cardiac excitation-contraction coupling: An iterated map study," Phys. Rev. E **75**, 011927 (2007).
[12] D. R. Chialvo, D. C. Michaels, and J. Jalife, "Supernormal excitability as a mechanism of chaotic dynamics of activation in cardiac purkinje fibers," Circ. Res. **66**, 525–545 (1990).
[13] N. F. Otani and J. R. F. Gilmour, "Memory models for the electrical properties of local cardiac systems," J. Theor. Biol. **187**, 409–436 (1997).
[14] J. R. F. Gilmour, N. F. Otani, and M. A. Watanabe, "Memory and complex dynamics in cardiac purkinje fibers," Am. J. Physiol. Heart Circ. Physiol. **272**, H1826 (1997).
[15] F. H. Fenton, S. J. Evans, and H. M. Hastings, "Memory in an excitable medium: A mechanism for spiral wave breakup in the low-excitability limit," Phys. Rev. Lett. **83**, 3964–3967 (1999).
[16] M. A. Watanabe and M. L. Koller, "Mathematical analysis of dynamics of cardiac memory and accommodation: Theory and experiment," Am. J. Physiol. Heart Circ. Physiol. **282**, H1534 (2002).
[17] K. Hall, D. J. Christini, M. Tremblay, J. J. Collins, L. Glass, and J. Billette, "Dynamic control of cardiac alternans," Phys. Rev. Lett. **78**, 4518–4521 (1997).
[18] M. J. Lab, "Mechanoelectric feedback (transduction) in heart: Concepts and implications," Cardiovasc. Res. **32**, 3–14 (1996).
[19] P. Kohl, P. Hunter, and D. Noble, "Stretch-induced changes in heart rate and rhythm: Clinical observations, experiments and mathematical models," Prog. Biophys. Mol. Biol. **71**, 91–138 (1999).
[20] P. Kohl and U. Ravens, "Cardiac mechano-electric feedback: Past, present, and prospect," Prog. Biophys. Mol. Biol. **82**, 3–9 (2003).
[21] T. A. Quinn, P. Kohl, and U. Ravens, "Cardiac mechano-electric coupling research: Fifty years of progress and scientific innovation," Prog. Biophys. Mol. Biol. **115**, 71–75 (2014).
[22] P. Kohl, A. Nesbitt, P. Cooper, and M. Lei, "Sudden cardiac death by commotio cordis: Role of mechano-electric feedback," Cardiovasc. Res. **50**, 280–289 (2001).
[23] W. Li, P. Kohl, and N. Trayanova, "Induction of ventricular arrhythmias following mechanical impact: A simulation study in 3D," J. Mol. Histol. **35**, 679–686 (2004).
[24] M. R. Franz, R. Cima, D. Wang, D. Profitt, and R. Kurz, "Electrophysiological effects of myocardial stretch and mechanical determinants of stretch-activated arrhythmias," Circulation **86**, 968–978 (1992).
[25] M. Zabel, B. S. Koller, F. Sachs, and M. R. Franz, "Stretch-induced voltage changes in the isolated beating heart: Importance of the timing of stretch and implications for stretch-activated ion channels," Cardiovasc. Res. **32**, 120–130 (1996).
[26] F. Ravelli, "Mechano-electric feedback and atrial fibrillation," Prog. Biophys. Mol. Biol. **82**, 137–149 (2003).
[27] M. R. Franz and F. Bode, "Mechano-electrical feedback underlying arrhythmias: The atrial fibrillation case," Prog. Biophys. Mol. Biol. **82**, 163–174 (2003).
[28] R. L. Chen, D. J. Penny, G. Greve, and M. J. Lab, "Stretch-induced regional mechanoelectric dispersion and arrhythmia in the right ventricle of anesthetized lambs," Am. J. Physiol. Heart Circ. Physiol. **286**, H1008–H1014 (2004).

[29]N. H. L. Kuijpers, R. H. Keldermann, H. M. M. ten Eikelder, T. Arts, and P. A. J. Hilbers, "The role of the hyperpolarization-activated inward current $I_f$ in arrhythmogenesis: A computer model study," IEEE Trans. Biomed. Eng. **53**, 1499–1511 (2006).
[30]N. H. L. Kuijpers, H. M. ten Eikelder, P. H. Bovendeerd, S. Verheule, T. Arts, and P. A. J. Hilbers, "Mechanoelectric feedback leads to conduction slowing and block in acutely dilated atria: A modeling study of cardiac electromechanics," Am. J. Physiol. Heart Circ. Physiol. **292**, H2832–H2853 (2007).
[31]K. Seo, M. Inagaki, S. Nishimura, I. Hidaka, M. Sugimachi, T. Hisada, and S. Sugiura, "Structural heterogeneity in the ventricular wall plays a significant role in the initiation of stretch-induced arrhythmias in perfused rabbit right ventricular tissues and whole heart preparations," Circ. Res. **106**, 176–184 (2010).
[32]S. C. Eijsbouts, M. Majidi, M. van Zandvoort, and M. A. Allessie, "Effects of acute atrial dilation on heterogeneity in conduction in the isolated rabbit heart," J. Cardiovasc. Electrophysiol. **14**, 269–278 (2003).
[33]Y. Hu, V. Gurev, J. Constantino, J. D. Bayer, and N. A. Trayanova, "Effects of mechano-electric feedback on scroll wave stability in human ventricular fibrillation," PLoS One **8**, e60287 (2013).
[34]U. Ravens, "Mechano-electric feedback and arrhythmias," Prog. Biophys. Mol. Biol. **82**, 255–266 (2003).
[35]T. A. Quinn, "The importance of non-uniformities in mechano-electric coupling for ventricular arrhythmias," J. Interv. Cardiac Electrophysiol. **39**, 25–35 (2014).
[36]I. R. Cantalapiedra, A. Peñaranda, L. Mont, J. Brugada, and B. Echebarria, "Reexcitation mechanisms in epicardial tissue: Role of $I_{to}$ density heterogeneities and $i_{Na}$ inactivation kinetics," J. Theor. Biol. **259**, 850–859 (2009).
[37]I. R. Cantalapiedra, A. Peñaranda, B. Echebarria, and J. Bragard, "Phase-2 reentry in cardiac tissue: Role of the slow calcium pulse," Phys. Rev. E **82**, 011907 (2010).
[38]T. Opthof, V. M. F. Meijborg, C. N. W. Belterman, and R. Coronel, "Synchronization of repolarization by mechano-electrical coupling in the porcine heart," Cardiovasc. Res. **108**, 181–187 (2015).
[39]F. Yapari, D. Deshpande, Y. Belhamadia, and S. Dubljevic, "Control of cardiac alternans by mechanical and electrical feedback," Phys. Rev. E **90**, 012706 (2014).
[40]A. Hazim, Y. Belhamadia, and S. Dubljevic, "Control of cardiac alternans in an electromechanical model of cardiac tissue," Comput. Biol. Med. **63**, 108–117 (2015).
[41]A. Hazim, Y. Belhamadia, and S. Dubljevic, "Mechanical perturbation control of cardiac alternans," Phys. Rev. E **97**, 052407 (2018).
[42]T. L. Riemer, E. A. Sobie, and L. Tung, "Stretch-induced changes in arrhythmogenesis and excitability in experimentally based heart cell models," Am. J. Physiol. **275**, H431–H442 (1998).
[43]N. Trayanova, W. Li, J. Eason, and P. Kohl, "Effect of stretch activated channels on defibrillation efficacy," Heart Rhythm **1**, 67–77 (2004).
[44]A. V. Panfilov, R. H. Keldermann, and M. P. Nash, "Self-organized pacemakers in a coupled reaction-diffusion-mechanics system," Phys. Rev. Lett. **95**, 258104 (2005).
[45]P. Kohl, C. Bollensdorff, and A. Garny, "Effects of mechanosensitive ion channels on ventricular electrophysiology: Experimental and theoretical models," Exp. Physiol. **91**, 307–321 (2006).
[46]T. Zeng, G. Bett, and F. Sachs, "Stretch-activated whole cell currents in adult rat cardiac myocytes," Am. J. Physiol. Heart Circ. Physiol. **278**, H548–H557 (2000).
[47]E. White, J.-Y. L. Guennec, J. M. Nigretto, F. Gannier, J. A. Argibay, and D. Garnier, "The effects of increasing cell length on auxotonic contractions; membrane potential and intracellular calcium transients in single guinea-pig ventricular myocytes," Exp. Physiol. **78**, 65–78 (1993).
[48]D. Kelly, L. Mackenzie, P. Hunter, B. Smaill, and D. Saint, "Gene expression of stretch-activated channels and mechanoelectric feedback in the heart," Clin. Exp. Pharmacol. Physiol. **33**, 642–648 (2006).
[49]A. Garny and P. Kohl, "Mechanical induction of arrhythmias during ventricular repolarization: Modeling cellular mechanisms and their interaction in two dimensions," Ann. N.Y. Acad. Sci. **1015**, 133–143 (2004).
[50]H. Hu and F. Sachs, "Stretch-activated ion channels in the heart," J. Mol. Cell. Cardiol. **29**, 1511–1523 (1997).
[51]S. M. Horner, D. J. Dick, C. F. Murphy, and M. J. Lab, "Cycle length dependence of the electrophysiological effects of increased load on the myocardium," Circulation **94**, 1131–1136 (1996).
[52]P. Taggart and M. Lab, "Cardiac mechano-electric feedback and electrical restitution in humans," Prog. Biophys. Mol. Biol. **97**, 452–460 (2008).
[53]C. Luo and Y. Rudy, "A model of the ventricular cardiac action potential. Depolarization, repolarization, and their interaction," Circ. Res. **68**, 1501–1526 (1991).
[54]M. P. Nash and A. V. Panfilov, "Electromechanical model of excitable tissue to study reentrant cardiac arrhythmias," Prog. Biophys. Mol. Biol. **85**, 501–522 (2004).
[55]S. A. Niederer, P. J. Hunter, and N. P. Smith, "A quantitative analysis of cardiac myocyte relaxation: A simulation study," Biophys. J. **90**, 1697–1722 (2006).
[56]L. E. Malvern, *Introduction to the Mechanics of a Continuous Medium* (Prentice-Hall Inc., Englewood Cliffs, NJ, 1969).
[57]J. Keener and J. Sneyd, *Mathematical Physiology* (Springer-Verlag, New York, 1998).
[58]R. H. Keldermann, M. P. Nash, H. Gelderblom, V. Y. Wang, and A. V. Panfilov, "Electromechanical wavebreak in a model of the human left ventricle," Am. J. Physiol. Heart Circ. Physiol. **299**, H134–H143 (2010).
[59]Z. QU, J. N. Weiss, and A. Garfinkel, "Cardiac electrical restitution properties and stability of reentrant spiral waves: A simulation study," Am. J. Physiol. Heart Circ. Physiol. **276**, H269–283 (1999).
[60]F. Xie, Z. Qu, J. Yang, A. Baher, J. N. Weiss, and A. Garfinkel, "A simulation study of the effects of cardiac anatomy in ventricular fibrillation," J. Clin. Invest. **113**, 686–693 (2004).
[61]Y. H. Zhang, J. B. Youm, H. K. Sung, S. H. Lee, S. Y. Ryu, W. K. Ho, and Y. E. Earm, "Stretch-activated and background non-selective cation channels in rat atrial myocytes," J. Physiol. **523**, 607–619 (2000).
[62]F. J. Vetter and A. D. McCulloch, "Mechanoelectric feedback in a model of the passively inflated left ventricle," Ann. Biomed. Eng. **29**, 414–426 (2001).
[63]W. Li, V. Gurev, A. D. McCulloch, and N. A. Trayanova, "The role of mechano-electric feedback in vulnerability to electric shock," Prog. Biophys. Mol. Biol. **97**, 461–478 (2008).
[64]W. Li, P. Kohl, and N. A. Trayanova, "Myocardial ischemia lowers precordial thump efficacy: An inquiry into mechanisms using three-dimensional simulations," Heart Rhythm **3**, 179–186 (2006).
[65]A. V. Panfilov, R. H. Keldermann, and M. P. Nash, "Drift and breakup of spiral waves in reaction-diffusion-mechanics systems," Proc. Natl. Acad. Sci. **104**, 7922–7926 (2007).
[66]T. L. Riemer and L. Tung, "Stretch-induced excitation and action potential changes of single cardiac cells," Prog. Biophys. Mol. Biol. **82**, 97–110 (2003).
[67]P. Kohl, K. Day, and D. Noble, "Cellular mechanisms of cardiac mechano-electric feedback in a mathematical model," Can. J. Cardiol. **14**, 111–119 (1998).
[68]K. Skouibine, N. Trayanova, and P. Moore, "A numerically efficient model for simulation of defibrillation in an active bidomain sheet of myocardium," Math. Biosci. **166**, 85–100 (2000).
[69]Z. Qu, A. Garfinkel, P. S. Chen, and J. N. Weiss, "Mechanisms of discordant alternans and induction of reentry in simulated cardiac tissue," Circulation **102**, 1664–1670 (2000).
[70]T. G. McNary, K. Sohn, B. Taccardi, and F. B. Sachse, "Experimental and computational studies of strain-conduction velocity relationships in cardiac tissue," Prog. Biophys. Mol. Biol. **97**, 383–400 (2008).
[71]J. J. Fox, J. L. McHarg, and J. R. F. Gilmour, "Ionic mechanism of electrical alternans," Am. J. Physiol. Heart Circ. Physiol. **282**, H516 (2002).
[72]F. G. Akar, K. R. Laurita, and D. S. Rosenbaum, "Cellular basis for dispersion of repolarization underlying reentrant arrhythmias," J. Electrocardiol. **33**, 23–31 (2000).
[73]C. S. Kuo, K. Munakata, C. P. Reddy, and B. Surawicz, "Characteristics and possible mechanism of ventricular arrhythmia dependent on the dispersion of action potential durations," Circulation **67**, 1356–1367 (1983).